Title: Translational control of *MPS1* links protein synthesis with the initiation of cell division and spindle pole body duplication in *Saccharomyces cerevisiae*

Authors: Heidi M. Blank[1], Annabel Alonso[2], Amy S. Fabritius[2], Mark Winey[2], Michael Polymenis[1]

Affiliations: [1]Department of Biochemistry and Biophysics, Texas A&M University, 2128 TAMU, College Station, TX 77843

[2]Department of Molecular and Cellular Biology, University of California Davis, Davis, CA 95616

Contact: mwiney@ucdavis.edu; polymenis@tamu.edu

Running Title: Translational control of *MPS1* in the cell cycle

Key words: SPB, MTOC, cell size, SIM, Start

ABSTRACT

Protein synthesis underpins cell growth and controls when cells commit to a new round of cell division at a point in late G1 of the cell cycle called Start. Passage through Start also coincides with the duplication of the microtubule-organizing centers, the yeast spindle pole bodies, which will form the two poles of the mitotic spindle that segregates the chromosomes in mitosis. The conserved Mps1p kinase governs the duplication of the spindle pole body in *Saccharomyces cerevisiae*. Here, we show that the *MPS1* transcript has a short upstream open reading frame that represses the synthesis of Mps1p. Mutating the *MPS1* uORF makes the cells smaller, accelerates the appearance of Mps1p in late G1, and promotes completion of Start. Monitoring the spindle pole body in the cell cycle using structured illumination microscopy revealed that mutating the *MPS1* uORF enabled cells to duplicate their spindle pole body earlier at a smaller cell size. The accelerated Start of *MPS1* uORF mutants depends on the G1 cyclin Cln3p and the transcriptional repressor Whi5p but not on the Cln1,2p G1 cyclins. These results identify growth inputs in mechanisms that control duplication of the microtubule-organizing center and implicate these processes in the coupling of cell growth with division.

INTRODUCTION

Basic cellular parameters, such as cell size and macromolecular composition, do not change much throughout successive cell divisions, and cell growth and division appear balanced (Polymenis 2022). The rate at which cells can divide usually depends not on how fast they can replicate their genome but on how fast they can synthesize everything else that goes into a newborn cell (Johnston *et al.* 1977). Newborn budding yeast daughter cells actively control when they begin replicating their genome in response to their growth status. They stay in the G1 phase of the cell cycle until they reach a characteristic threshold of cell growth known as critical size (Hartwell and Unger 1977; Di Talia *et al.* 2007). The protein synthesis rate is thought to underpin overall cell growth and determine when cells will reach their critical size and commit to a new round of DNA replication at Start (Polymenis and Aramayo). Translational control of *CLN3*, encoding a G1 cyclin, alters the timing of Start in different nutrients (Polymenis and Schmidt 1997; Blank *et al.* 2018), and synthesis of Cln3p in G1 may respond to a critical rate of protein synthesis (Litsios *et al.* 2019). However, other molecular targets that could impose the protein synthesis requirements for cell division initiation have remained elusive.

The spindle pole body (SPB) of yeast is a large protein organelle serving the same role as the centrosome in animals. The two SPBs in mitosis form the poles from which all the microtubules of the mitotic spindle originate (Jaspersen and Winey 2004). The SPB is a stack of three major protein layers or plaques embedded in the nuclear envelope. Besides the chromosomes, the SPB is the only large macromolecular complex present in a single copy early in the G1 phase of the cell cycle. When cells pass through Start, a protein extension of the middle plaque called the half-bridge nucleates the new SPB formation, maturing and separating from the old SPB. From classical experiments involving loss-of-function mutants, it is thought

that passage through Start is required for SPB duplication and not vice versa (Hartwell *et al.* 1974; Pringle 1981).

Mps1p is a conserved protein serine, threonine, and tyrosine kinase required for SPB duplication (Winey *et al.* 1991; Lauzé *et al.* 1995; Liu and Winey 2012). Mps1p also regulates various other mitotic events, most prominently bipolar chromosome attachment and the spindle checkpoint (Liu and Winey 2012). Post-translational mechanisms control Mps1p's levels (through proteolysis), activity (through phosphorylation by several kinases, including by Mps1p itself), and localization (at least in part through phosphorylation and localized degradation) in the cell (Liu and Winey 2012). Mps1p abundance is very low, at ~500 molecules/cell in asynchronous cells (Ho *et al.* 2018). Mps1p levels peak in metaphase, consistent with Mps1p's numerous mitotic roles, but then the anaphase-promoting complex destroys Mps1p for a timely mitotic exit (Palframan *et al.* 2006). Over-expression of Mps1p arrests cells in mitosis (Hardwick *et al.* 1996). How Mps1p levels are controlled in G1 is unknown.

We previously identified *MPS1* as one of a few mRNAs whose translational efficiency changes in the cell cycle (Blank *et al.* 2017). Here, we identify a short upstream open reading frame (uORF) in *MPS1*. Mutating the *MPS1* uORF caused an earlier appearance of Mps1p in G1 and accelerated SPB duplication. It also reduced the critical size for Start completion in a Cln3p-dependent manner. These results reveal direct growth and protein synthesis inputs in the Mps1p-controlled SPB cycle. They also show that SPB-related processes can actively determine when cells commit to a new round of cell division at Start.

MATERIALS AND METHODS

Key resources table

Where known, the Research Resource Identifiers (RRIDs) are shown.

Reagent type (species) or resource	Designation	Source or reference	Identifiers	Additional information
antibody	Peroxidase Anti-Peroxidase (PAP) Soluble Complex	Sigma-Aldrich	P1291	(1:1000)
antibody	Anti-Pgk1p antibody, rabbit polyclonal	Novex by Life Technologies	459250	(1:1000)
antibody	Alexa Fluor® 488 AffiniPure Goat Anti-Mouse IgG (H+L)	Jackson Immunoresearch Laboratories	115-545-003	(1:1500)
chemical compound, drug	Dextrose	Sigma-Aldrich	D9434	
chemical compound, drug	Zymolyase 20T	MP biomedicals	SKU 08320921	
chemical compound, drug	Tris (hydroxymethyl) aminomethane	Sigma-Aldrich	252859	
chemical compound, drug	Tris base	Roche	TRIS-RO	
chemical compound, drug	Sodium chloride	Sigma-Aldrich	S7653	
chemical compound, drug	Magnesium chloride hexahydrate	USP	1374248	
chemical compound, drug	DTT	Sigma-Aldrich	D0632	
chemical	Triton™ X-100	Sigma-Aldrich	T8787	

compound, drug				
chemical compound, drug	Phosphate buffered saline (PBS)	Sigma-Aldrich	P4417	
chemical compound, fixation	Paraformaldehyde, 16%	Ted Pella, Inc.	18505	SIM microscopy
Commercial assay, kit	One step RT-ddPCR Advanced kit for probes	Bio-Rad	1864021	RNA surveillance
other	BioTrace™ NT nitrocellulose	Pall Corporation	66485	Immunoblotting
other	Immobilon®-FL membrane	MilliporeSigma	IPFL07810	Immunoblotting
other	Mini-PROTEAN® TGX Stain-Free™ Gels, 4-15%	Bio-Rad	4568086	Immunoblotting
other	Yeast extract	Sigma-Aldrich	Y1625	
other	Peptone	Sigma-Aldrich	P5905	
other	Glass beads	Scientific Industries	SI-BG05	
other	ProLong™ Gold Antifade Mountant	ThermoFisher Scientific	P36934	SIM microscopy
Sequence based reagent	IV403709-F1			TCTGGAGAATTCTTTTCAAA ATATAACATTTCAAAAATAAA CGACAAAAACACTGAATACC GGATCCCCGGGTTAATTAA
Sequence based reagent	IV403709-R1			AAATTGTGGCATCACAGTAA TGCTCAAACAAAAACTTTAAT GTTCTTTACTCTTTTAGGGG AATTCGAGCTCGTTTAAAC
Sequence based reagent	IV403783-FWD			CAACAAATGGTGATTCTGGA G
Sequence based reagent	IV403164-REV			TGGGAAAGTAAAGCTGATCC G
Sequence based reagent	pBS1539	(Puig et al)		C- terminal TAP fusion plasmid
Sequence based reagent	AT-17TA-MPS1-R EV			CTCGATTTTAAATCCACATAA TCATGGAATGAGTTTGTTGA

				CATGTTTGTTTTGAGATCTAC CAGTTCTTGCAGAAAC
Sequence based reagent	uORFm2-MPS1-REV			GAGTTTGTTGACATGTTTGT TTTGAGATTTTTCAGTTCTTG CAGAAACAATTTATTATTTTG GTTGTAAAGCTACTTCTATAA ACAACTGCAATATTCCTATTC
Sequence based reagent	IV403783-FWD			CAACAAATGGTGATTCTGGA G
Sequence based reagent	IV403638-FWD			CATGTTTATATATTCTGACCA
Sequence based reagent	IV403164-REV			TGGGAAAGTAAAGCTGATCC G
Sequence based reagent	IV403783-FWD			CAACAAATGGTGATTCTGGA G
Sequence based reagent	MPS1-CTAP-FWD			GATGATCTCAATGATGTGGT AGACACTGTTTTAAGGAAAT TTGCAGATTACAAAATTTCCA TGGAAAAGAGAAG
Sequence based reagent	MPS1-CTAP-REV			AAACTCTAAATGTATTTATGT TCATAACTGGCACATGCTTTT CTTCCTTATGCGGCTCTTTA CGACTCACTATAGGG
Sequence based reagent	MPS1-FAM-probe	Sc04106277_s1, Cat#4448892	Thermo Fisher Scientific	RNA surveillance
Sequence based reagent	UBC6-VIC-probe	Sc04118595_s1, Cat# 4351372	Thermo Fisher Scientific	RNA surveillance
software, algorithm	AccuComp Z2	Beckman Coulter	383550	Software to monitor number and size of cells with Z2 cell counter
Software, algorithm	QuantaSoft™ Software	Bio-Rad		Software to determine the concentration of transcript abundance by ddPCR
software, algorithm	ImageJ	https://imagej.net/	RRID:SCR_003070	Image processing software
software, algorithm	Adobe Photoshop	https://www.adobe.com/products/photoshop.html	RRID:SCR_014199	Image processing software
software, algorithm	RStudio	http://www.rstudio.com/	RRID:SCR_000432	Software for the R statistical computing environment
software,	SGD	http://www.yeastg	RRID:SCR_00	Saccharomyces Genome

algorithm		enome.org/	4694	Database
software, algorithm	R	https://www.r-project.org	v3.6.3 RRID:SCR_001905	Statistical Computing Environment
strain, strain background (S. cerevisiae)	BY4743	(Giaever et al., 2002)	RRID:SCR_003093	MATa/α his3Δ1/his3Δ1 leu2Δ0/leu2Δ0 LYS2/lys2Δ0 met15Δ0/MET15 ura3Δ0/ura3Δ0
strain, strain background (S. cerevisiae)	BY4741	(Giaever et al., 2002)	RRID:SCR_003093	MATa his3Δ1 leu2Δ0 met15Δ0 ura3Δ0
strain, strain background (S. cerevisiae)	BY4741	Horizon Discovery TAP tagged ORF collection	Catalog ID:YSC1178-202230172	MATa his3Δ1 leu2Δ0 met15Δ0 ura3Δ0 MPS1-TAP::HIS3MX6
strain, strain background (S. cerevisiae)	W303a			MATa leu2-3,112 trp1-1 can1-100 ura3-1 ade2-1 his3-11,15
strain, strain background (S. cerevisiae)	W303	This study (HB68)	Horizon strain backcrossed 3x to W303	MATa leu2-3,112 TRP+ can1-100 ura3-1 ADE2+ his3-11,15, MPS1-TAP::HIS3MX6
strain, strain background (S. cerevisiae)	W303	This study (HB67)	Horizon strain backcrossed 3x to W303	MATα leu2-3,112 TRP+ can1-100 ura3-1 ADE2+ his3-11,15, MPS1-TAP::HIS3MX6
strain, strain background (S. cerevisiae)	BY4741	This study (HB48)		MATa his3Δ1 leu2Δ0 met15Δ0 ura3Δ0 KanMX-uORFm1-MPS1-TAP::URA3
strain, strain background (S. cerevisiae)	W303	This study (HB53)	HB48 backcrossed 3x to W303	MATα leu2-3,112 trp1-1 can1-100 ura3-1 ADE2+ his3-11,15 KanMX-uORFm1-MPS1-TAP::URA3
strain, strain background (S. cerevisiae)	W303	This study (uORFm1-MPS; HB49)	HB48 backcrossed 3x to W303	MATa leu2-3,112 trp1-1 can1-100 ura3-1 ADE2+ his3-11,15 KanMX-uORFm1-MPS1-TAP::URA3
strain, strain background (S. cerevisiae)	W303	This study (uORFm2-MPS1; HB219)		MATa leu2-3,112 trp1-1 can1-100 ura3-1 ade2-1 his3-11,15

				KanMX-uORFm2-MPS1-TAP::URA3
strain, strain background (S. cerevisiae)	W303	This study (HB99)	HB67 x MWY5264	MATa leu2-3,112 TRP+ can1-100 ura3-1 ADE2+ his3-11,15 MPS1-TAP::HIS SPC42-GFP::KanMX SPC110-tomato::HIS3
strain, strain background (S. cerevisiae)	W303	This study (HB263)	HB53 x MWY5264	MATa leu2-3,112 trp1-1 can1-100 ura3-1 ADE2+ his3-11,15 KanMX-uORFm1-MPS1-TAP::URA3 SPC42-GFP::KanMX SPC110-tomato::HIS3
strain, strain background (S. cerevisiae)	W303	Winey lab collection	MWY5264	MATα leu2-3,112 trp1-1 can1-100 ura3-1 ADE2+ his3-11,15 SPC42-GFP::KanMX SPC110-tomato::HIS3
strain, strain background (S. cerevisiae)	BY4741	This study (HB173, HB176)	HB48 x cln3Δ::kanMX	MATa his3Δ1 leu2Δ0 met15Δ0 ura3Δ0 cln3Δ::kanMX kanMX-uORFm1-MPS1-TAP::URA3
strain, strain background (S. cerevisiae)	BY4741	This study (HB177)	MPS1-TAP-HISMX6 x cln3Δ::kanMX	MATa his3Δ1 leu2Δ0 met15Δ0 ura3Δ0 cln3Δ::kanMX MPS1-TAP::HIS3MX
strain, strain background (S. cerevisiae)	BY4741	This study (HB169, HB170)	MPS1-TAP-HIS3MX6 x whi5Δ::kanMX	MATa his3Δ1 leu2Δ0 met15Δ0 ura3Δ0 whi5Δ::KanMX MPS1-TAP::HIS3MX6
strain, strain background (S. cerevisiae)	BY4741	This study (HB174, HB175)	HB48 x whi5Δ::kanMX	MATa his3Δ1 leu2Δ0 met15Δ0 ura3Δ0 whi5Δ::kanMX KanMX6-uORFm1-MPS1-TAP::URA3
strain, strain background (S. cerevisiae)	BY4743	This study (MSP238)		KanMX-MPS1/MPS1, BY4743 otherwise
strain, strain background (S. cerevisiae)	BY4743	This study (MSP239)		KanMX-uORFm1-MPS1/MPS1, BY4743 otherwise
strain, strain background (S. cerevisiae)	BY4741	This study (MSP240-3C)		KanMX-MPS1, BY4741 otherwise
strain, strain background (S.	BY4741	This study (MSP241-1C)		KanMX-uORFm1-MPS1, BY4741 otherwise

cerevisiae)				
strain, strain background (S. cerevisiae)	BY4741	This study (HB278, HB279, HB280)	MSP47 x HB275	cln1Δ::KanMX cln2Δ::URA3 uORF+ MPS1-TAP::HIS, BY4741 otherwise
strain, strain background (S. cerevisiae)	BY4741	This study (HB281)	MSP47 x HB276	cln1Δ::KanMX cln2Δ::URA3 uORFm1 MPS1-TAP::URA

Strains and media

All the strains used in this study are shown in the Key Resources Table above. Unless noted otherwise, the cells were cultivated in the standard, rich, undefined medium YPD (1% $^{w}/_{v}$ yeast extract, 2% $^{w}/_{v}$ peptone, 2% $^{w}/_{v}$ dextrose), at 30°C (Kaiser *et al.* 1994).

To modify the *MPS1*-5' leader, we first inserted a *KanMX6* cassette upstream, at position ChrIV:403709 with the PCR-mediated methodology of (Longtine *et al.* 1998), using primers IV403709-F1 and IV403709-R1 (see Key Resources Table). The PCR product was introduced into strain BY4743, generating the heterozygous strain MSP238, which was sporulated and dissected to generate the haploid MATα (MSP240-3A) and MATa (MSP240-3C) segregants. The *KanMX6* insertion was verified by PCR, using primers IV403783-FWD and IV403164-REV.

To introduce the uORFm1 mutation, we used primers IV403783-FWD and AT-17TA-MPS1-REV in a PCR reaction with genomic DNA from MSP240-3A. The PCR product was then used to transform strain BY4743, generating strain MSP239. The introduction of the uORFm1 was initially verified by restriction digestion since the uORFm1 introduces a BglII restriction site. Strain MSP239 was then sporulated and dissected to generate the haploid uORFm1 haploid MATa (MSP240-1C) segregant. The uORFm1 mutation was verified by sequencing with primers IV403638-FWD and IV403164-REV.

To insert a C-terminal TAP tag at the *MPS1* locus, we amplified the TAP-tagged sequences from plasmid pBS1539 (Puig *et al.* 2001) with primers MPS1-CTAP-FWD and MPS1-CTAP-REV and used the PCR product to transform the above generated *uORF*$^{+}$*-MPS1* and *uORFm1-MPS1* haploid strains. These BY4741-based strains were then crossed with W303α three times to generate the equivalent W303-based strains.

For constructing the uORFm2-MPS1-TAP strain, primers uORFm2-MPS1-REV and IV403783-FWD were used in a PCR reaction, using as template genomic DNA of a uORFm1-MPS1-TAP strain. The generated PCR product contained the KanMX cassette and introduced the point mutations at the uORF of *MPS1* shown in Figure 1. This PCR product was transformed into W303a cells, and potential candidates were sequenced with primers IV403638-FWD and IV403164-REV to confirm the presence of the uORF mutations. Verified uORFm2 strains were then transformed again with the PCR product of primer pair MPS1-CTAP-FWD and MPS1-CTAP-REV with DNA extracted from the uORFm1 strain to insert the TAP protein tag. All transformed strains were backcrossed once.

We constructed the fluorescently tagged strains for SIM microscopy by crossing strain MWY5624 with the strains carrying the appropriate TAP-tagged *uORF+-MPS1* or *uORFm1-MPS1* allele. Since these crosses involved multiple genes tagged with the same marker, the obtained tetrads were analyzed carefully to pick non-parental ditypes of the double genetic markers. Strains were further confirmed by immunoblotting for Mps1p-TAP, and both fluorescent markers were confirmed microscopically.

Sample-size and replicates

For sample-size estimation, no explicit power analysis was used. All the replicates in every experiment shown were biological ones from independent cultures. A minimum of three

biological replicates was analyzed in each case, as indicated in each corresponding figure's legends. Where three replicates were the minimum number of samples analyzed, the robust bootstrap ANOVA was used to compare different populations via the t1waybt function, and the posthoc tests via the mcppb20 function of the WRS2 R language package (Wilcox 2011; Mair and Wilcox 2020). We used nonparametric statistical methods for measurements where at least four independent replicates were analyzed, as indicated in each case. No data or outliers were excluded from any analysis.

Centrifugal elutriation and cell size measurements

For each elutriation experiment in YPD (1% $^{w}/_{v}$ yeast extract, 2% $^{w}/_{v}$ peptone, 2% $^{w}/_{v}$ dextrose, plus 0.02 g/L of adenine for strains of W303 background), a 350 mL culture was allowed to reach a density of 1-5E+07 cells/mL. Cells were loaded at a 35 mL/min pump speed onto a large elutriator chamber (40 mL), spinning at 3,200 rpm (Beckman J-6M/E centrifuge). The centrifuge chamber was set at 4°C during all centrifugation steps until approximately 10 min before cell harvesting, when the temperature was increased to avoid the refrigeration from turning on and disrupting the cell gradient in the chamber. For typical time-series experiments with synchronous elutriated cultures (e.g., see Figure 2A), we isolated the first, early G1 daughter fraction and monitored it at regular intervals afterward as it progressed in the cell cycle, as we have described elsewhere (Hoose *et al.* 2012; Soma *et al.* 2014).

Protein surveillance

Protein extracts for immunoblots were made with the sodium hydroxide extraction method described previously (Amberg *et al.* 2006). The extracts from synchronous culture samples were run on 10% Tris-Glycine SDS–PAGE gels and transferred to a nitrocellulose membrane. For

detection of proteins of interest on immunoblots, we used an anti-Pgk1p antibody to detect Pgk1p and the peroxidase-anti-peroxidase (PAP) soluble complex to detect TAP-tagged proteins. Chemiluminescence reagents were from Thermo Scientific and used at the dilutions recommended by the manufacturer for detection of the TAP-tagged Mps1p. A secondary antibody was used to detect Pgk1p (Jackson Immunoresearch Laboratories). Detection of the proteins was digitally acquired using an Amersham™ Imager 600 (GE Healthcare).

The extracts from batch cultures were prepared the same as above but instead ran on Mini-PROTEAN® TGX Stain-Free™ Gels and transferred to a low-fluorescence PVDF membrane. Protein detection was as above, but using the stain-free gel technology, we could acquire a total protein image of the blot to be used as an additional loading control along with Pgk1p. The manufacturer's instructions were followed to activate the gel, except using an Amersham™ Imager (GE Healthcare) for 3 minutes to activate the gel after completion of electrophoresis. Following transfer to an Immobilon®-FL membrane, the total protein was detected using the UV channel of the Amersham™ Imager 600. Images were processed with the "Subtract Background" tool, and band intensities quantified using the "Measure" tool to obtain a mean intensity for each band, using the ImageJ software package. The area measured was kept constant for a particular sample series for each blot analyzed.

To calculate the Log2(expressed ratios) in cell cycle series (e.g., see Figure 2), for any one protein of interest (Mps1p-TAP or Pgk1p), each signal value was divided by the average signal across the entire cell cycle series for that protein. These ratios were then Log2-transformed and reported on the y-axis.

Transcript abundance using digital droplet PCR (ddPCR)

For RNA surveillance, RNA extracts were made as described previously (Blank *et al.* 2020). Briefly, RNA was extracted using the hot acidic phenol method. Cell pellets were resuspended in 0.4 ml of TES buffer (10 mM Tris, pH 7.5; 10 mM EDTA, and 0.5% SDS) with 0.1 ml of glass beads. Then, 0.4 ml of acid phenol, pH 4.5, was added, and the samples were heated at 65°C for 0.5 h with occasional vortexing for 10 s each time. The samples were then centrifuged for 5 m at 13,000 g. The aqueous layer was transferred to a new tube containing 1 ml of cold 100% ethanol with 40 µl of 3 M sodium acetate and incubated overnight at 4°C. The next day, the samples were centrifuged at 13,000 g for 20 min at 4°C, washed with 80% ethanol, and centrifuged again for 5 min at 13,000 g. The pellets were resuspended in 25 µl water. The amount of total RNA in each sample was measured with a ThermoFisher NanoDrop™ spectrophotometer. For the quantification of transcript abundance, 1 ng of total RNA was used for each sample.

The ddPCR reaction mixture was prepared by following the manufacturer's protocol (One-Step RT-ddPCR Advanced Kit for Probes), using the TaqMan® hydrolysis probes labeled with FAM-MBP for MPS1 and VIC-MBP for UBC6 reporter fluorophores. The mixture was kept on ice throughout the whole experiment. Once the reaction mixture was prepared, the samples were placed into a droplet generator (QX200™ AutoDG™ Droplet Digital™ PCR System), which uses specially developed reagents and microfluidics to partition each sample into 20,000 nl-sized droplets. Once the droplets were generated, the samples were transferred to a thermal cycler (C1000 Touch™ Thermal cycler) for PCR. Following the PCR, the plate containing the droplets was placed in a droplet reader (Bio-Rad, QX200 Droplet reader). he droplet reader's autosampler picks up droplets from each of the wells of the PCR plate, and fluorescence is measured for individual droplets. The abundance of the transcripts was obtained using the

QuantaSoft™ Software. Transcript levels of *MPS1* were normalized against the corresponding transcript levels of *UBC6*.

Cell fixation for SIM microscopy

Cells containing the fluorescent markers for SPB analysis were elutriated as described earlier. For each time point, 1 mL of cell culture was collected, pelleted, and washed in 1mL of PBS. Cells were then spun at 3,000rpm for 3 m in a microcentrifuge and resuspended in 1mL of 4% paraformaldehyde (Ted Pella, Inc.) in a 133mM sucrose in PBS solution. Fixation was for 15 min at room temperature, followed by two more washes in PBS. Cells were stored at 4°C until they were analyzed by microscopy.

SIM microscopy

Structured Illumination Microscopy analysis was performed on fixed cells, which had been mounted onto glass slides using ProLong Gold Antifade mountant (ThermoFisher Scientific). Mounted cells were stored in the dark at room temperature for 48 h prior to SIM analysis. Images of Z-series (step size of 0.2 μm) of cells were collected using the Nikon Structured Illumination Super-Resolution Microscope fitted with a 100×1.46 NA objective. Images were captured in the 3D-SIM mode using NIS-Elements and SIM processing was performed using the SIM module in the Nikon software package. Image projections were made in Image-J software (National Institutes of Health).

In vitro phosphorylation assays. All methods for protein purification and kinase reactions have been described previously (Venta *et al.* 2020). Ndc80p (1-257 aa) and Sic1p (1-215 aa) were expressed and purified as 6xHis fusions. Sic1p-AP had all known Cdk sites mutated to

Ala. Whi5p, Cdc31p, and Spc29p were expressed and purified as GST fusions of the full-length protein in each case. In Figure S5A, the enzyme concentration was 2 nM, and the substrate protein was 1 μM. In the experiments in Figure S5B, Mps1p was present at 4.2 nM, and the protein substrates were at 350 nM. After SDS -PAGE, gels were vacuum-dried. The BAS-IP MS 2040 E screen, Biomolecular Imager Typhoon 5, and ImageQuant TL software (all from Amersham) were used for autoradiography.

RESULTS AND DISCUSSION

Mutating a conserved uORF in *MPS1* reduces cell size

To test the role of translational control in Mps1p synthesis, we looked at possible *cis*-elements in the *MPS1* mRNA that could mediate that control. The 5'-leader of *MPS1* is 133 nt-long (Poch *et al.* 1994) and has a uORF (Figure S1, top). The uORF initiates 17 nt upstream but overlaps and terminates past the main *MPS1* start codon (Figure S1). The uORF could repress the translation of *MPS1* because ribosomes that synthesize the uORF-encoded peptide will bypass the *MPS1* start codon. A uORF at the same position, albeit of varying length and sequence, is present in other *Saccharomyces* genomes (Figure S1). Based on aggregate ribosome profiling experiments from the literature, the uORF sequences are bound by ribosomes (Michel *et al.* 2014), suggesting that the uORF is translated.

To test the role of the *MPS1* uORF, we mutated its start codon in two ways (Figure 1A). The 5'-leader may also be structured (Figure S2A). The uORF mutations we introduced may (*uORFm1-MPS1*) or not (*uORFm2-MPS1*) alter the predicted 5'-leader structure (Figure S2A). The two different mutants provide independent means to test the role of the *MPS1* uORF. We introduced these mutations in their native context in the chromosome, with the endogenous *MPS1* promoter driving the *MPS1* mRNA expression (see Materials and Methods). We also introduced a C-terminal TAP tag to visualize Mps1p-TAP on immunoblots (see Materials and Methods).

While both *MPS1* uORF mutants proliferated at the same rate as their *uORF*$^{+}$ counterpart, they had a small overall cell size, regardless of strain background (BY4741 in Figure 1B; W303 - Figure 1C). The cells were born at the right size (Figure 1C, left panel), but the mean size of asynchronously proliferating cells was about 10-15% smaller (Figure 1C, right panel; $p<0.005$ based on the non-parametric Kruskal-Wallis and the posthoc Nemenyi tests).

The uORF mutations did not change the steady-state levels of *MPS1* mRNA or Mps1-TAP protein in asynchronous cells (Figure S2B). This is not surprising due to the other known mechanisms regulating Mps1p abundance in the cell cycle, as described in the next section. However, the smaller mean cell size of asynchronous cultures of the *MPS1* uORF mutants was suggestive of cell cycle-dependent phenotypes, which we examined next.

Mutating the *MPS1* uORF accelerates the appearance of Mps1p in the cell cycle and promotes Start

Smaller cell size is often associated with accelerated completion of Start, as shown initially for stabilized, gain-of-function mutants of the G1 cyclin Cln3p (Sudbery *et al.* 1980; Cross 1988). To measure the timing of Start in the *MPS1* uORF mutants, we obtained highly synchronous cultures by centrifugal elutriation, which maintains as much as possible the coordination of cell growth with division (Creanor and Mitchison 1979; Aramayo and Polymenis 2017). The abundance of Mps1p in elutriated daughter cells has not been measured in past studies. We found that Mps1p-TAP is absent in G1 and begins accumulating at the G1/S transition when cells begin budding (Figure 2A, top panel). This is expected because Mps1p is a substrate of the anaphase-promoting complex (APC) (Palframan *et al.* 2006), and the APC is active in G1. Mps1p-TAP levels peak late in the cell cycle, in mitosis, when the percentage of budded cells is the highest (>90%), and then Mps1 levels drop again as cells exit mitosis (Figure 2A, B). In both independently constructed *MPS1* uORF mutants, Mps1p-TAP abundance was also periodic, absent in G1, and peaking late in the cell cycle (Figure 2A, B). However, Mps1p-TAP began appearing in smaller cells (~5 fL smaller) in the *MPS1* uORF mutants than wild-type cells (Figure 2A, B). Hence, although mutating the *MPS1* uORF does not change the steady-state

levels of Mps1p in asynchronous cells (Figure S2B), it changes the kinetics of the Mps1p appearance in the cell cycle (Figure 2).

Budding yeast daughter cells commit to a new round of DNA replication when they reach a critical size threshold at Start. Since budding coincides with the initiation of DNA replication in yeast (Hartwell *et al.* 1974), from such synchronous elutriated cultures, the critical size is commonly defined as the size at which half the cells are budded. Remarkably, the critical size of *MPS1* uORF mutants was ~40 fL, while that of wild type cells was >45 fL (Figure 2C; e.g., the critical size is reduced by 9% (Wilcoxon rank-sum test; p-value = 0.0005828) in the *uORFm1-MPS1* mutant). We conclude that Start was accelerated in the *MPS1* uORF mutants.

Reducing the translational efficiency of *MPS1* accelerates SPB duplication in synchronous, elutriated cells.

Since Mps1p plays multiple roles in SPB duplication, we examined the effect of the *uORFm1-MPS1* mutation on the timing of morphological landmarks of the SPB cycle. Note that cells continue to grow during a cell cycle block, and when they are released from their arrest, they typically progress quickly through the G1 phase of the cycle. In contrast, early G1 cells obtained by centrifugal elutriation are not arrested and must meet their growth requirements for Start. Hence, synchronous cultures obtained by centrifugal elutriation enable monitoring of early G1 events. To our knowledge, the SPB cycle has not been followed in elutriated synchronous cultures starting in early G1.

We used a strain harboring two fluorescently tagged SPB components, *Spc42p-GFP* and *Spc110p-tomato*, to visualize SPB duplication's early steps. Spc42p is a central plaque component of the SPB (Bullitt *et al.* 1997), which Mps1p phosphorylates (Castillo *et al.* 2002). Mps1p also phosphorylates Spc110p, an inner plaque SPB component, which attaches γ-tubulin

to the SPB (Friedman *et al.* 2001). Early G1 cells of this strain were obtained by elutriation and monitored at regular intervals for cell size and budding, and samples were fixed for SPB analysis by structured illumination microscopy (SIM) (Figure 3). The single SPB has a half-bridge attached, which doubles in length once SPB duplication commences (Li *et al.* 2006). Once the half-bridge elongates, proteins assemble at the distal end of the bridge to form a precursor to a new SPB called a satellite (Winey and Bloom 2012). Spc42p is one of several proteins deposited at the satellite location. This event is viewed as a cone-like structure flaring off the original SPB, denoted as 'satellite-early' in Figure 3. When most of the cells are unbudded, the prominent SPB feature seen is one SPB alone or one SPB with a small cone process, indicating early satellite body formation (Figure 3). Shortly before the size at which budding occurs in *uORF*$^{+}$*-MPS1* cells, fully formed satellite processes are detected, denoted as 'satellite-late' in Figure 3. The appearance of duplicated, side-by-side SPBs is detected once the cells bud and pass through Start (Figure 3; (Byers and Goetsch 1974)). The final step, the separation of the SPBs, occurs during the anaphase of mitosis, which is consistent with our data showing this separation occurring near the end of the cell cycle (Figure 3). These data describe the morphology of early events of the SPB cycle in highly synchronous, elutriated newborn daughter cells, documenting the formation of early satellite structures soon after birth.

We introduced the *uORFm1-MPS1* allele in the *SPC42-GFP*, *SPC110-tomato* strain and measured the timing of the above event of the SPB cycle. Using cell size as a proxy for cell cycle position, the early steps of the SPB occur at the same time in the *uORFm1-MPS1* mutant and *uORF*$^{+}$*-MPS1* cells. For example, the appearance of cells with satellite-late morphology peaks at 40 fL in both strains (Figure 3A). However, *uORFm1-MPS1* cells peak with SPB duplicated morphology soon after, at a size of ~42 fL. In contrast, the *uORF*$^{+}$*-MPS1* cells do so at a larger cell size (47-48 fL, compare the second-row panels in Figure 3A). The subsequent

cell separation step is also accelerated in *uORFm1-MPS1* cells compared to *uORF*$^{+}$*-MPS1* ones (Figure 3A, compare the two top panels). These results show that cells that do not have the *MPS1* uORF duplicate their SPB earlier, at a smaller size, consistent with an accelerated completion of Start.

The accelerated Start of *MPS1* uORF mutants depends on Cln3p and Whi5p, but not on Cln1,2p

We then asked if *uORFm1-MPS1* functionally interacts with known regulators of Start. In yeast, two critical regulators of Start are the G1 cyclin Cln3p (promotes Start) and Whi5p (inhibits Start). Whi5p is a transcriptional repressor, analogous to the retinoblastoma (Rb) gene product of animal cells (Costanzo *et al.* 2004; de Bruin *et al.* 2004). Direct, localized phosphorylation of RNA PolII by the Cln3p-Cdc28p kinase complex triggers transcription of >100 genes at Start, including transcription of *CLN1* and *CLN2*, encoding G1/S cyclins (Kõivomägi *et al.* 2021). Removing Cln3p makes the cells bigger (Cross 1988; Nash *et al.* 1988), while removing Whip5 makes them smaller (Costanzo *et al.* 2004; de Bruin *et al.* 2004). Cells lacking Whi5p are among the smallest-sized mutants in yeast (Jorgensen *et al.* 2002). Introducing the *uORFm1-MPS1* allele in *whi5Δ* cells made them smaller (Figure 4A). On the other hand, mutating the *MPS1* uORF did not reduce the size of *cln3Δ* cells (Figure 4A). Lastly, Cln3p levels in the cell cycle did not change in *uORFm1-MPS1* mutants (Figure S3).

To better gauge the dependence of Mps1p on G1/S regulators, we measured the timing of Start in synchronous, elutriated cultures. The critical size threshold for Start is greatly increased in cells lacking Cln3p (at 80 fL, compared to 46 fL for wild type cells; Figure 4B), and it was not affected at all in double, *uORFm1-MPS1, cln3Δ* mutants (Figure 4B). Likewise, despite their smaller size (Figure 4A), *uORFm1-MPS1, whi5Δ* mutants did not have a reduced

critical size at START (Figure 4B). A caveat in the analysis of the critical size of *whi5Δ* cells is that these mutants have such a small critical size, so a further reduction by de-repressing translation of *MPS1* may be difficult to impose. These results suggest that Cln3p, and possibly Whi5p, are needed for Mps1p to accelerate Start when the *MPS1* uORF is mutated.

We also measured Start kinetics in cells lacking both the Cln1p and Cln2p G1 cyclins. Double *cln1,2Δ* mutants have a much larger critical size (at ~71 fL, compared to 46 fL for wild type cells; Figure 5A). De-repressing translation of *MPS1*, in *uORFm1-MPS1, cln1,2Δ* cells, significantly reduced critical size (~60 fL; Figure 5A). We also noticed that loss of Cln1,2p dampened the cell cycle-dependent oscillation of Mps1p (Figure 5B, C), but it was restored in *uORFm1-MPS1, cln1,2Δ* cells (Figure 5B, C). Nonetheless, despite the smaller amplitude in the changing levels of Mps1 in the cell cycle in *cln1,2Δ* cells, these results suggest that de-repressing translation of *MPS1* accelerates Start mostly independently of Cln1,2p.

Since Cdk is known to phosphorylate Mps1p at T29 (Jaspersen *et al.* 2004), it is possible that phosphorylation of Mps1p by G1/Cdk somehow promotes the G1/S transition. To test this idea, we measured the critical size of the non-phosphorylatable *MPS1-T29A* mutant. There was no difference in the critical size of *MPS1-T29A* mutant cells and their otherwise wild type counterparts (Figure S4). These data suggest that the Cdk-dependent phosphorylation of Mps1 does not significantly affect the timing of Start. Instead, Mps1p may promote Start by phosphorylating some G1/S regulators. We tested this possibility in vitro, asking if Mps1p could phosphorylate Whi5p or Sic1p (Figure S5). Sic1p is an inhibitor of B-type cyclin/Cdk complexes, whose phosphorylation triggers its degradation, enabling DNA replication to commence (Venta *et al.* 2020). Indeed, in vitro, Mps1p phosphorylated both Sic1p and Whi5p (Figure S5A). However, Mps1p's kinase activity towards Sic1p and Whi5p was lower than that of Cln2/Cdk and Clb5p/Cdk towards these substrates (Figure S5A). We then examined the ability of Mps1p

to phosphorylate Whi5p and Sic1p compared to other known Mps1p substrates with roles in SPB duplication (Cdc31p and Spc29p) or the spindle assembly checkpoint (Ndc80p). The Mps1p activity toward Sic1p and Whi5p was comparable to its activity against Cdc31p but 2-3-fold lower than its activity against Ndc80p and Spc29p (Figure S5B). Furthermore, Mps1p could target Sic1p even when all known Cdk phosphorylation sites on Sic1p were mutated to alanine (Sic1p-AP; see Figure S5B), presumably at other non-Cdk sites. Although it is currently unclear how Mps1p exercises its role in the timing of Start in cells, our in vitro data argue that Mps1p could potentially phosphorylate Start regulators (Figure S5). In such a scenario, Mps1p role may be secondary to Cdk or other kinases, helping to bring about this critical cellular transition, possibly through its broad specificity as a kinase. We note that, in a perhaps analogous manner, Mps1p ensures that the spindle assembly checkpoint is established, participating in the phosphorylation of outer kinetochore proteins following the action of the Aurora-B kinase (Liu and Winey 2012).

Conclusions

The role of centrosomes in cell division is as old as the chromosome theory of heredity, with centrosome amplification a common feature of cancers (Boveri 2008). Normally, centrosome and SPB duplication are entrained with the master cell cycle switch governed by the activity of cyclin-dependent kinase (Cdk) (Jaspersen and Winey 2004; Nigg and Raff 2009). However, in some cases, they can duplicate independently of cell-cycle progression (Nigg and Raff 2009). In animals, autonomous oscillations of the polo-like kinase Plk4 can drive centrosome duplication independently of Cdk (Aydogan *et al.* 2020). Intriguingly, centriole growth in the cell cycles of fly embryos appears to follow a homeostatic ‘sizer-like’ model, actively monitoring and adjusting their growth until they reach the proper size (Aydogan *et al.* 2018). An analogous mechanism

has not been shown for the budding yeast SPB. However, the same principle operates during the G1 phase of daughter cells to control Cdk activity before cells commit at Start to initiate budding and DNA replication (Hartwell and Unger 1977; Di Talia *et al.* 2007). Our results argue that through translational control of *MPS1*, growth and protein synthesis also directly trigger SPB duplication, expanding the range of growth inputs the cell uses to control the timing of Start (Figure 6). Hence, monitoring the growth and duplication of the SPB/centrosome may contribute to the overall coupling of cell growth with division in proliferating cells.

DATA AVAILABILITY

Strains and plasmids are available upon request. The authors affirm that all data necessary for confirming the conclusions of the article are present within the article, figures, and tables.

FUNDING

This work was supported by NIH grants R01 GM123139 to M.P., P01 GM105537 to M.W.. A.A. was supported by NIH T32 Oncogenic Signals and Chromosome Biology Training grant (T32 CA108459).

ACKNOWLEDGEMENTS

We thank the MCB Light Microscopy Imaging Facility at the University of California - Davis. We also thank Dr. Mart Loog (University of Tartu, Estonia) for the in vitro kinase assays.

REFERENCES

Amberg D. C., D. J. Burke, and J. N. Strathern, 2006 Yeast protein extracts. CSH Protoc. 2006: pdb.prot4152. https://doi.org/10.1101/pdb.prot4152

Aramayo R., and M. Polymenis, 2017 Ribosome profiling the cell cycle: lessons and challenges. Curr Genet 63: 959–964. https://doi.org/10.1007/s00294-017-0698-3

Aydogan M. G., A. Wainman, S. Saurya, T. L. Steinacker, A. Caballe, *et al.*, 2018 A homeostatic clock sets daughter centriole size in flies. J. Cell Biol. 217: 1233–1248. https://doi.org/10.1083/jcb.201801014

Aydogan M. G., T. L. Steinacker, M. Mofatteh, Z. M. Wilmott, F. Y. Zhou, *et al.*, 2020 An Autonomous Oscillation Times and Executes Centriole Biogenesis. Cell 181: 1566-1581.e27. https://doi.org/10.1016/j.cell.2020.05.018

Blank H. M., R. Perez, C. He, N. Maitra, R. Metz, *et al.*, 2017 Translational control of lipogenic enzymes in the cell cycle of synchronous, growing yeast cells. EMBO J 36: 487–502. https://doi.org/10.15252/embj.201695050

Blank H. M., M. Callahan, I. P. E. Pistikopoulos, A. O. Polymenis, and M. Polymenis, 2018 Scaling of G1 Duration with Population Doubling Time by a Cyclin in Saccharomyces cerevisiae. Genetics 210: 895–906. https://doi.org/10.1534/genetics.118.301507

Blank H. M., O. Papoulas, N. Maitra, R. Garge, B. K. Kennedy, *et al.*, 2020 Abundances of transcripts, proteins, and metabolites in the cell cycle of budding yeast reveal coordinate control of lipid metabolism. Mol. Biol. Cell 31: 1069–1084. https://doi.org/10.1091/mbc.E19-12-0708

Boveri T., 2008 Concerning the origin of malignant tumours by Theodor Boveri. Translated and annotated by Henry Harris. J. Cell Sci. 121: 1–84.

Bruin R. A. de, W. H. McDonald, T. I. Kalashnikova, J. Yates 3rd, and C. Wittenberg, 2004 Cln3

activates G1-specific transcription via phosphorylation of the SBF bound repressor Whi5. Cell 117: 887–98. https://doi.org/10.1016/j.cell.2004.05.025

Bullitt E., M. P. Rout, J. V. Kilmartin, and C. W. Akey, 1997 The yeast spindle pole body is assembled around a central crystal of Spc42p. Cell 89: 1077–1086. https://doi.org/10.1016/s0092-8674(00)80295-0

Byers B., and L. Goetsch, 1974 Duplication of spindle plaques and integration of the yeast cell cycle. Cold Spring Harb. Symp. Quant. Biol. 38: 123–131. https://doi.org/10.1101/sqb.1974.038.01.016

Castillo A. R., J. B. Meehl, G. Morgan, A. Schutz-Geschwender, and M. Winey, 2002 The yeast protein kinase Mps1p is required for assembly of the integral spindle pole body component Spc42p. J. Cell Biol. 156: 453–465. https://doi.org/10.1083/jcb.200111025

Cherry J. M., E. L. Hong, C. Amundsen, R. Balakrishnan, G. Binkley, *et al.*, 2012 Saccharomyces Genome Database: the genomics resource of budding yeast. Nucleic Acids Res 40: D700-5. https://doi.org/10.1093/nar/gkr1029

Costanzo M., J. L. Nishikawa, X. Tang, J. S. Millman, O. Schub, *et al.*, 2004 CDK activity antagonizes Whi5, an inhibitor of G1/S transcription in yeast. Cell 117: 899–913. https://doi.org/10.1016/j.cell.2004.05.024

Creanor J., and J. Mitchison, 1979 Reduction of perturbations in leucine incorporation in synchronous cultures of Schizosaccharomyces pombe made by elutriation. J. Gen. Microbiol. 112: 385–388.

Cross F. R., 1988 DAF1, a mutant gene affecting size control, pheromone arrest, and cell cycle kinetics of Saccharomyces cerevisiae. Mol Cell Biol 8: 4675–84.

Di Talia S., J. M. Skotheim, J. M. Bean, E. D. Siggia, and F. R. Cross, 2007 The effects of molecular noise and size control on variability in the budding yeast cell cycle. Nature

448: 947–51. https://doi.org/10.1038/nature06072

Friedman D. B., J. W. Kern, B. J. Huneycutt, D. B. Vinh, D. K. Crawford, *et al.*, 2001 Yeast Mps1p phosphorylates the spindle pole component Spc110p in the N-terminal domain. J. Biol. Chem. 276: 17958–17967. https://doi.org/10.1074/jbc.M010461200

Gruber A. R., R. Lorenz, S. H. Bernhart, R. Neuböck, and I. L. Hofacker, 2008 The Vienna RNA websuite. Nucleic Acids Res. 36: W70-74. https://doi.org/10.1093/nar/gkn188

Hardwick K. G., E. Weiss, F. C. Luca, M. Winey, and A. W. Murray, 1996 Activation of the budding yeast spindle assembly checkpoint without mitotic spindle disruption. Science 273: 953–956. https://doi.org/10.1126/science.273.5277.953

Hartwell L. H., J. Culotti, J. R. Pringle, and B. J. Reid, 1974 Genetic control of the cell division cycle in yeast. Science 183: 46–51.

Hartwell L. H., and M. W. Unger, 1977 Unequal division in Saccharomyces cerevisiae and its implications for the control of cell division. J Cell Biol 75: 422–35.

Ho B., A. Baryshnikova, and G. W. Brown, 2018 Unification of Protein Abundance Datasets Yields a Quantitative Saccharomyces cerevisiae Proteome. Cell Syst 6: 192-205.e3. https://doi.org/10.1016/j.cels.2017.12.004

Hoose S. A., J. A. Rawlings, M. M. Kelly, M. C. Leitch, Q. O. Ababneh, *et al.*, 2012 A systematic analysis of cell cycle regulators in yeast reveals that most factors act independently of cell size to control initiation of division. PLoS Genet. 8: e1002590. https://doi.org/10.1371/journal.pgen.1002590

Jaspersen S. L., and M. Winey, 2004 The budding yeast spindle pole body: structure, duplication, and function. Annu Rev Cell Dev Biol 20: 1–28. https://doi.org/10.1146/annurev.cellbio.20.022003.114106

Jaspersen S. L., B. J. Huneycutt, T. H. Giddings, K. A. Resing, N. G. Ahn, *et al.*, 2004

Cdc28/Cdk1 regulates spindle pole body duplication through phosphorylation of Spc42 and Mps1. Dev. Cell 7: 263–274. https://doi.org/10.1016/j.devcel.2004.07.006

Johnston G. C., J. R. Pringle, and L. H. Hartwell, 1977 Coordination of growth with cell division in the yeast Saccharomyces cerevisiae. Exp Cell Res 105: 79–98.

Jorgensen P., J. L. Nishikawa, B. J. Breitkreutz, and M. Tyers, 2002 Systematic identification of pathways that couple cell growth and division in yeast. Science 297: 395–400. https://doi.org/10.1126/science.1070850

Kaiser C., S. Michaelis, A. Mitchell, and Cold Spring Harbor Laboratory., 1994 *Methods in yeast genetics : a Cold Spring Harbor Laboratory course manual*. Cold Spring Harbor Laboratory Press, Cold Spring Harbor, NY.

Kõivomägi M., M. P. Swaffer, J. J. Turner, G. Marinov, and J. M. Skotheim, 2021 Localized phosphorylation of RNA Polymerase II by G1 cyclin-Cdk promotes cell cycle entry. bioRxiv 2021.03.25.436872. https://doi.org/10.1101/2021.03.25.436872

Lauzé E., B. Stoelcker, F. C. Luca, E. Weiss, A. R. Schutz, *et al.*, 1995 Yeast spindle pole body duplication gene MPS1 encodes an essential dual specificity protein kinase. EMBO J. 14: 1655–1663.

Li S., A. M. Sandercock, P. Conduit, C. V. Robinson, R. L. Williams, *et al.*, 2006 Structural role of Sfi1p-centrin filaments in budding yeast spindle pole body duplication. J. Cell Biol. 173: 867–877. https://doi.org/10.1083/jcb.200603153

Litsios A., D. H. E. W. Huberts, H. M. Terpstra, P. Guerra, A. Schmidt, *et al.*, 2019 Differential scaling between G1 protein production and cell size dynamics promotes commitment to the cell division cycle in budding yeast. Nat. Cell Biol. 21: 1382–1392. https://doi.org/10.1038/s41556-019-0413-3

Liu X., and M. Winey, 2012 The MPS1 family of protein kinases. Annu Rev Biochem 81:

561–85. https://doi.org/10.1146/annurev-biochem-061611-090435

Longtine M. S., A. McKenzie 3rd, D. J. Demarini, N. G. Shah, A. Wach, *et al.*, 1998 Additional modules for versatile and economical PCR-based gene deletion and modification in Saccharomyces cerevisiae. Yeast 14: 953–61. https://doi.org/10.1002/(SICI)1097-0061(199807)14:10<953::AID-YEA293>3.0.CO;2-U

Mair P., and R. Wilcox, 2020 Robust statistical methods in R using the WRS2 package. Behav. Res. Methods 52: 464–488. https://doi.org/10.3758/s13428-019-01246-w

Michel A. M., G. Fox, A. M. Kiran, C. De Bo, P. B. F. O'Connor, *et al.*, 2014 GWIPS-viz: development of a ribo-seq genome browser. Nucleic Acids Res. 42: D859–D864. https://doi.org/10.1093/nar/gkt1035

Nash R., G. Tokiwa, S. Anand, K. Erickson, and A. B. Futcher, 1988 The WHI1+ gene of Saccharomyces cerevisiae tethers cell division to cell size and is a cyclin homolog. EMBO J 7: 4335–46.

Nigg E. A., and J. W. Raff, 2009 Centrioles, centrosomes, and cilia in health and disease. Cell 139: 663–678. https://doi.org/10.1016/j.cell.2009.10.036

Palframan W. J., J. B. Meehl, S. L. Jaspersen, M. Winey, and A. W. Murray, 2006 Anaphase Inactivation of the Spindle Checkpoint. Science 313: 680–684. https://doi.org/10.1126/science.1127205

Poch O., E. Schwob, F. de Fraipont, A. Camasses, R. Bordonne, *et al.*, 1994 RPK1, an essential yeast protein kinase involved in the regulation of the onset of mitosis, shows homology to mammalian dual-specificity kinases. Mol Gen Genet 243: 641–53.

Polymenis M., and E. V. Schmidt, 1997 Coupling of cell division to cell growth by translational control of the G1 cyclin CLN3 in yeast. Genes Dev 11: 2522–31.

Polymenis M., 2022 *Two from One: A Short Introduction to Cell Division Mechanisms*. John

Wiley & Sons.

Polymenis M., and R. Aramayo, Translate to divide: control of the cell cycle by protein synthesis. Microb. Cell 2: 94–104. https://doi.org/10.15698/mic2015.04.198

Pringle J. R. Hartwell, L. H., 1981 The Saccharomyces cerevisiae Cell Cycle, pp. 97–142 in *The Molecular and Cellular Biology of the Yeast Saccharomyces*, Cold Spring Harbor Laboratory Press, Cold Spring Harbor, New York.

Puig O., F. Caspary, G. Rigaut, B. Rutz, E. Bouveret, *et al.*, 2001 The tandem affinity purification (TAP) method: a general procedure of protein complex purification. Methods 24: 218–29. https://doi.org/10.1006/meth.2001.1183

Soma S., K. Yang, M. I. Morales, and M. Polymenis, 2014 Multiple metabolic requirements for size homeostasis and initiation of division in Saccharomyces cerevisiae. Microb. Cell 1: 256–266. https://doi.org/10.15698/mic2014.08.160

Sudbery P. E., A. R. Goodey, and B. L. Carter, 1980 Genes which control cell proliferation in the yeast Saccharomyces cerevisiae. Nature 288: 401–4.

Venta R., E. Valk, M. Örd, O. Košik, K. Pääbo, *et al.*, 2020 A processive phosphorylation circuit with multiple kinase inputs and mutually diversional routes controls G1/S decision. Nat. Commun. 11: 1836. https://doi.org/10.1038/s41467-020-15685-z

Wilcox R. R., 2011 *Introduction to robust estimation and hypothesis testing*. Academic press.

Winey M., L. Goetsch, P. Baum, and B. Byers, 1991 MPS1 and MPS2: novel yeast genes defining distinct steps of spindle pole body duplication. J. Cell Biol. 114: 745–754. https://doi.org/10.1083/jcb.114.4.745

Winey M., and K. Bloom, 2012 Mitotic spindle form and function. Genetics 190: 1197–1224. https://doi.org/10.1534/genetics.111.128710

FIGURES

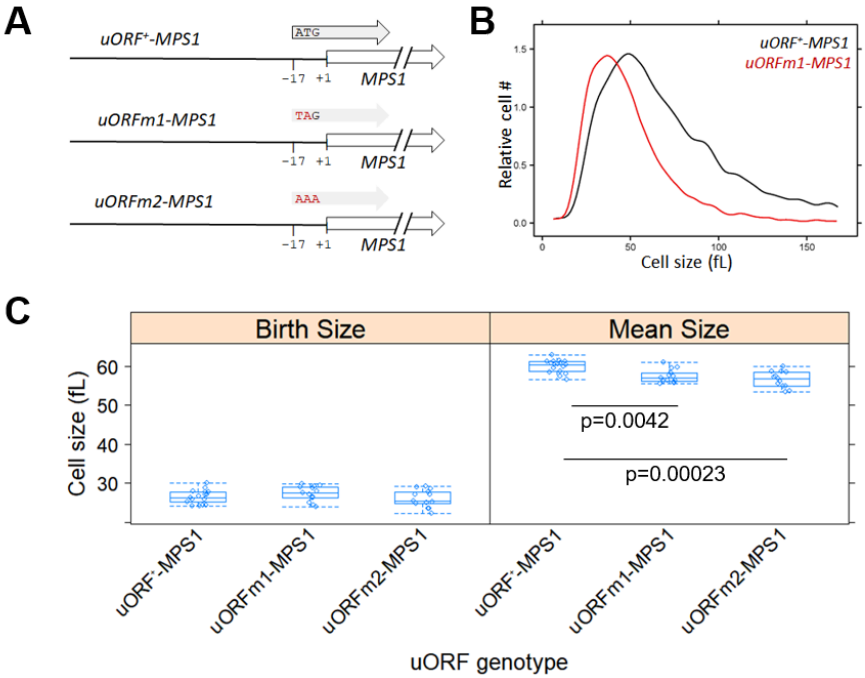

Figure 1. Mutating a conserved uORF in *MPS1* reduces cell size. A, Schematic of the *MPS1* locus in the strains used in this study to test the role of the *MPS1* uORF. **B**, Cell size histograms (size in fL, x-axis; number of cells, y-axis) for the indicated strains (*uORF*$^{+}$*-MPS1* [strain MSP240-3C] and *uORFm1-MPS1* [strain MSP241-1C]; see Materials and Methods) in otherwise wild type cells, cultured in rich medium (YPD), proliferating asynchronously and exponentially. **C**, Box-plots showing the mean and birth size of populations of cells from multiple independent measurements from the indicated strains (all in the W303 background, carrying TAP-tagged *MPS1* alleles; see Materials and Methods). The associated p-values were from the nonparametric Kruskal-Wallis and the posthoc Nemenyi tests (calculated with the PMCMR R language package) between the samples shown. The values used to generate the graphs in C are in supplementary File1/sheet 'fig1c'.

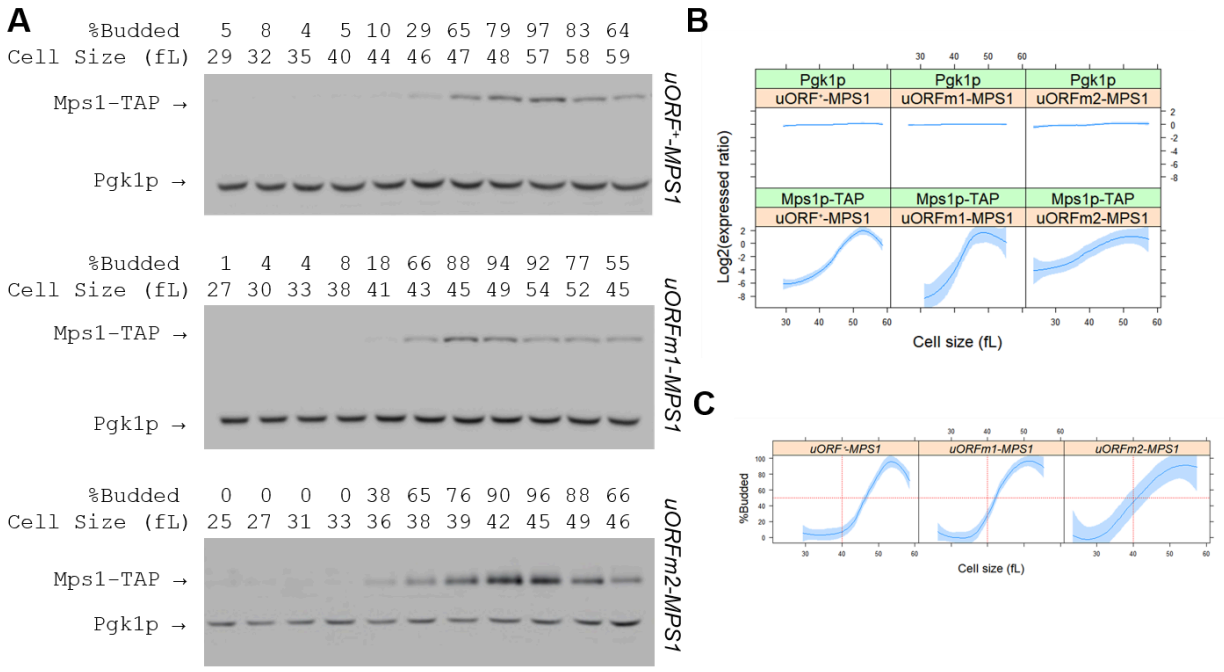

Figure 2. Mutating the *MPS1* uORF accelerates the appearance of Mps1p in the cell cycle and promotes Start. The abundance of Mps1p-TAP was monitored in wild type and *uORFm-MPS1* cells, constructed as described in Materials and Methods. Samples were collected by elutriation in a rich, undefined medium (YPD) and allowed to progress synchronously in the cell cycle. Experiment-matched loading controls (measuring Pgk1p abundance) were also quantified and shown in parallel. **A**, Representative immunoblots, along with the percentage of budded cells (%B) and the cell size (in fL), for each of the samples. **B**, From at least three independent experiments in each case, the Mps1p-TAP and Pgk1p signal intensities were quantified as described in Materials and Methods. The Log2(expressed ratios) values are on the y-axis, and cell size values are on the x-axis. Loess curves and the standard errors at a 0.95 level are shown. All the immunoblots for this figure are in supplementary File2, while the values used to generate the graphs are in supplementary File1/sheet 'fig2b' and sheet 'fig2c'.

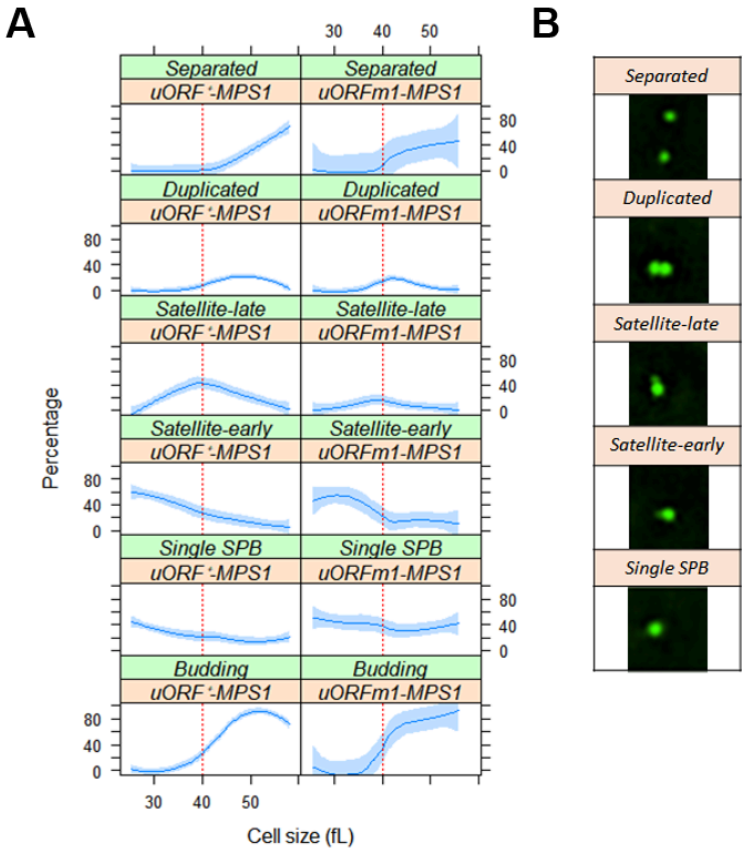

FIGURE 3. Reducing the translational efficiency of *MPS1* accelerates SPB duplication in synchronous, elutriated cells. A, Elutriated, early G1 daughter cells of the indicated *MPS1* uORF genotype carrying *SPC42-GFP* and *SPC110-tomato* alleles were monitored by SIM microscopy as they progressed synchronously in the cell cycle, in rich (YPD) medium. On the x-axis of each panel is cell size. On the y-axis is the percentage of cells with the indicated morphology, based on the fluorescence of SPB markers. Loess curves and the standard errors at a 0.95 level are shown. **B**, Representative SIM images of the SPB morphology, based on Spc42-GFP fluorescence, used to score the synchronous cells at various stages of the cell cycle. The values used to generate the graphs are in supplementary File1/sheet 'fig3a'.

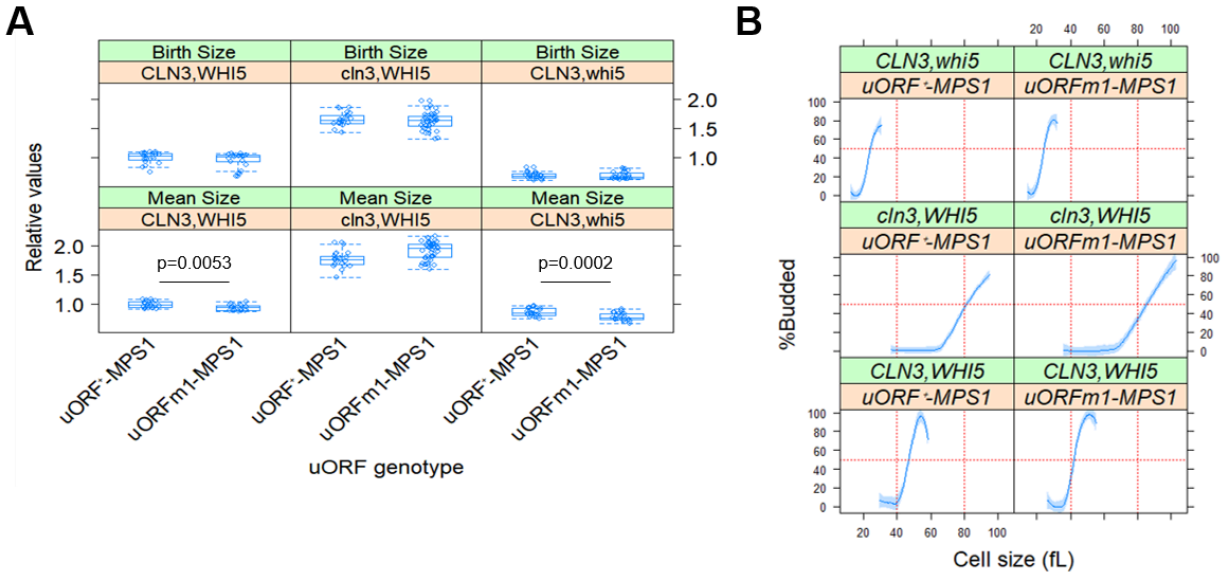

FIGURE 4. The smaller critical size of *MPS1* uORF mutants depends on the G1 cyclin Cln3p and the transcriptional repressor Whi5p. A, Box-plots showing the mean and birth size of populations of cells from multiple independent measurements from the indicated strains. The associated p-values from the non-parametric Wilcoxon rank-sum test between the two samples in each case are shown. **B**, Summary of cell cycle profiles of the indicated *MPS1* uORF genotype and strain background, done as in Figure 2. Loess curves and the standard errors at a 0.95 level are shown. The critical size is reduced by 9% (Wilcoxon rank sum test; p-value = 0.0005828) in *uORFm1-MPS1* cells, but there is no effect in *cln3Δ* and *whi5Δ* cells. The values used to generate the graphs are in supplementary File1/sheet 'fig4a' and sheet 'fig4b'.

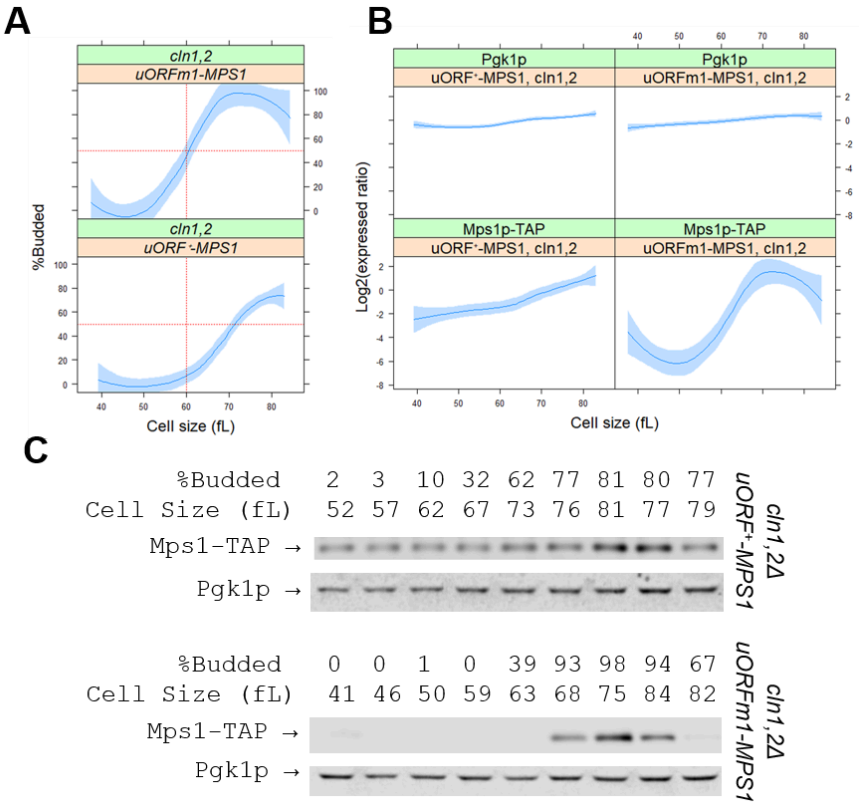

FIGURE 5. Translational de-repression of Mps1p accelerates Start in cells lacking Cln1p and Cln2p. A, Summary of cell cycle profiles of double *cln1,2Δ* mutants, of the indicated *MPS1* uORF genotype background, done as in Figures 2&3. Loess curves and the standard errors at a 0.95 level are shown. The critical size is reduced by at least 10 fL in *uORFm1-MPS1* cells. The values used to generate the graphs are in supplementary File1/sheet 'fig5a'. **B**, The amplitude of the Mps1p-TAP oscillation in the cell cycle is smaller in *cln1,2Δ* mutants, but it is restored when mutating the *MPS1* uORF. The abundance of Mps1p-TAP was monitored as in Figure 2. **C**, Representative immunoblots, along with the percentage of budded cells (%B) and the cell size (in fL), for each of the samples. All the immunoblots for this figure are in supplementary File4, while the values used to generate the graphs are in supplementary File1/sheet 'fig5a' and sheet 'fig5b'.

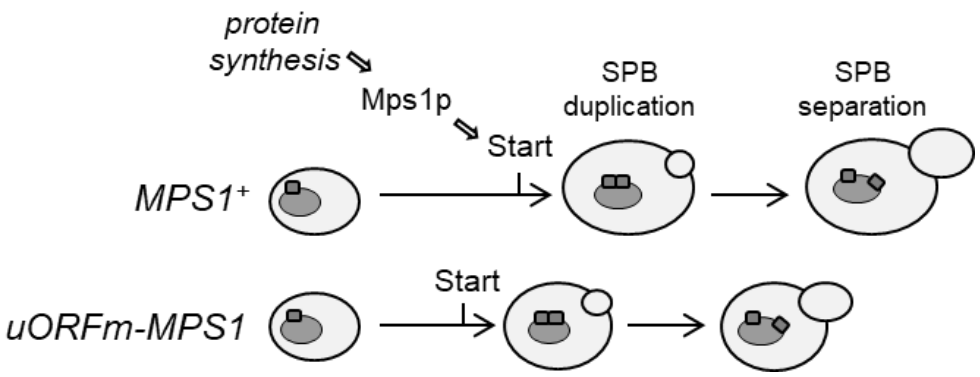

Figure 6. Schematic overview of our findings, connecting protein synthesis to Start and SPB duplication processes via translational regulation of *MPS1*.

```
                 uORF        M  I  S  K  Q  T  C  Q  Q  T  H  S  M  I  M  W  I  *
                Mps1p                          M  S  T  N  S  F  H  D  Y  V  D  L  K  S  R  T
  SGD_Scer_MPS1/YDL028C     TGGATGATCTCAAAACAAACATGTCAACAAACTCATTCCATGATTATGTGGATTTAAAATCGAGAAC
                            -17             +1

                 uORF        M  T  S  K  Q  S  C  Q  Q  I  H  S  M  I  I  W  I  *
                Mps1p                          M  S  T  N  S  F  H  D  Y  M  D  L  K  S  R  T
     MIT_Spar_c96_3651      TGAATGACCTCAAAACAATCATGTCAACAAATTCATTCCATGATTATATGGATTTAAAGTCGAGAAC

                 uORF        M  S  S  I  *
                Mps1p                          M  S  T  N  S  F  H  D  Y  M  D  S  K  S  R  M
    MIT_Suva_c788_3655      TGAATGAGTTCAATATAATTATGTCAACAAATTCATTCCATGACTATATGGATTCAAAGTCGAGAAC

                 uORF        M  S  S  I  *
                Mps1p                          M  S  T  N  S  F  H  D  Y  M  D  S  K  S  R  M
 WashU_Sbay_Contig554.19    TGAATGAGTTCAATATAATTATGTCAACAAATTCATTCCATGACTATATGGATTCAAAGTCGAGAAC

                 uORF        M  S  S  K  K  L  C  R  Q  I  H  S  M  T  I  W  I  Q  N  R  K  *
                Mps1p                          M  S  T  N  S  F  H  D  Y  M  D  S  K  S  K  M
 WashU_Skud_Contig1646.3    TGAATGAGCTCCAAAAAATTATGTCGACAAATTCATTCCATGACTATATGGATTCAAAATCGAAAAT
```

Figure S1. The initiation position of a uORF in the *MPS1* transcript, but not the length or the sequence of the uORF-encoded peptide, is conserved in the *Saccharomyces* genus. The genomic DNA sequence for *S. cerevisiae* (top) and for the related species are shown (as listed on the Saccharomyces Genome Database (SGD) fungal sequence alignments (Cherry *et al.* 2012)). Above each DNA sequence, the sequences of the uORF-encoded peptides and the amino-terminal sequence of Mps1p are shown.

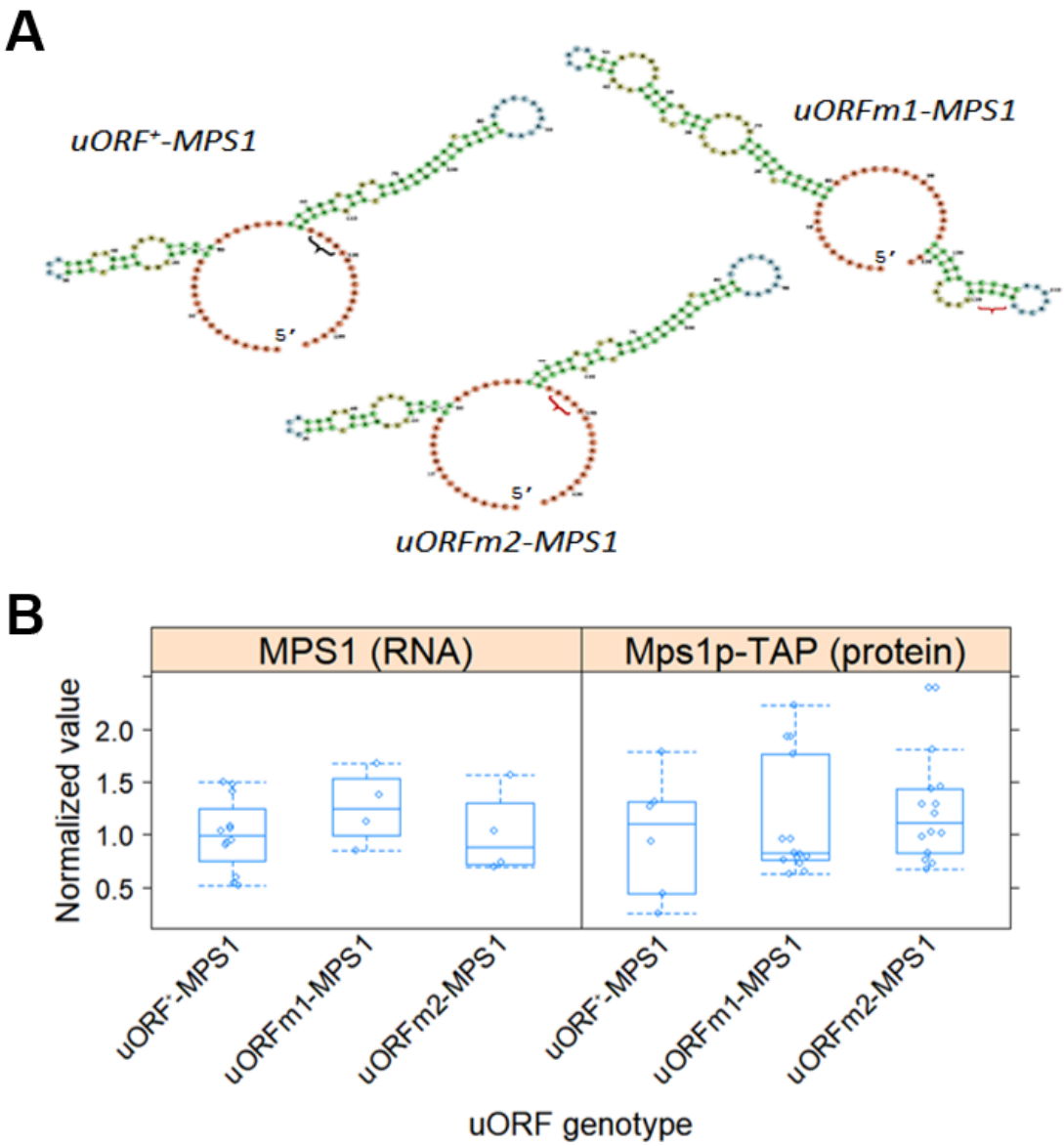

Figure S2. Mutating the *MPS1* uORF does not significantly change the steady-state abundance of Mps1p in asynchronous cells. A, Predicted RNA structure of the *MPS1* 5'-leader in each of the strains shown. The predicted structures were the minimum free energy (MFE) ones calculated with the Vienna RNA Websuite (Gruber *et al.* 2008). The brackets indicate the position of the start codon of the uORF in each case. **B**, Mutating the *MPS1* uORF does not significantly change the steady-state abundance of Mps1p in asynchronous cells. The

box-plots show the levels of *MPS1* mRNA (left panel) and Mps1p protein (right panel) from multiple independent experiments, measured as described in Materials and Methods. The values were normalized against both Pgk1p levels in each sample and total protein, using the Mini-PROTEAN® TGX Stain-Free™ Gels, as described in Materials and Methods. All the immunoblots for this figure are in supplementary File3, while the values used to generate the graphs are in supplementary File1/sheet ‘figs2b’.

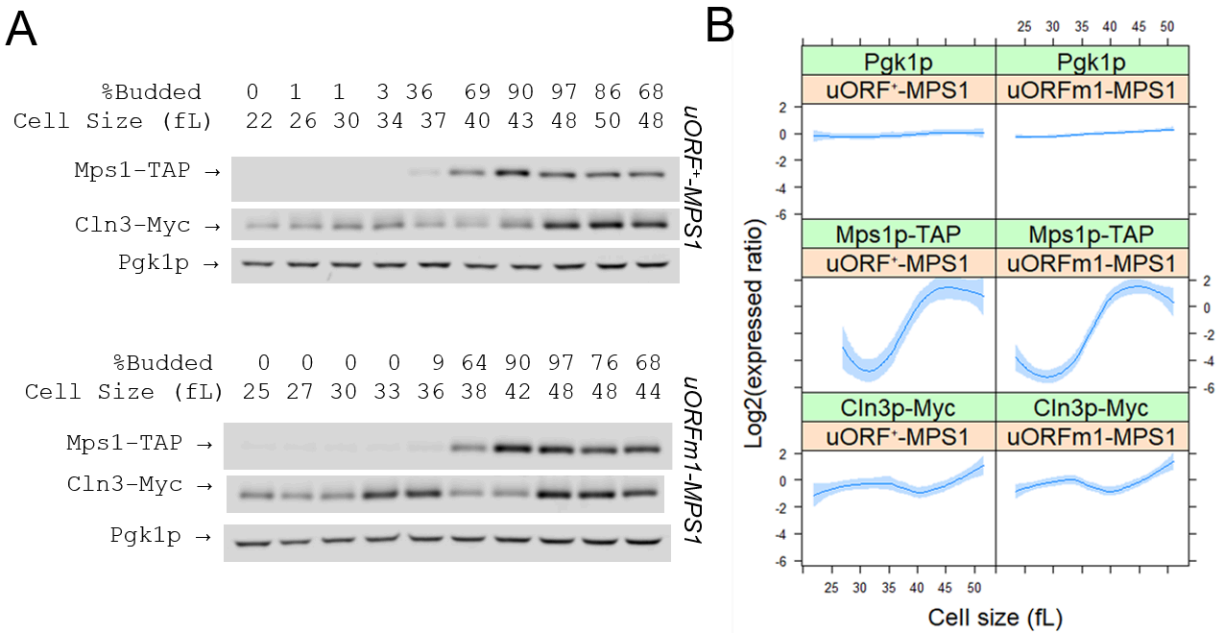

Figure S3. Translational de-repression of Mps1p does not change Cln3p levels in the cell cycle. The abundance of the indicated proteins was monitored in wild type and *uORFm-MPS1* cells, constructed as described in Materials and Methods. Samples were collected by elutriation in a rich, undefined medium (YPD) and allowed to progress synchronously in the cell cycle. Experiment-matched loading controls (measuring Pgk1p abundance) were also quantified and shown in parallel. **A**, Representative immunoblots, along with the percentage of budded cells (%B) and the cell size (in fL), for each of the samples. **B**, From at least three independent experiments in each case, the Mps1p-TAP, Cln3-Myc, and Pgk1p signal intensities were quantified as described in Materials and Methods. The Log2(expressed ratios) values are on the y-axis, and cell size values are on the x-axis. Loess curves and the standard errors at a 0.95 level are shown. All the immunoblots for this figure are in supplementary File5, while the values used to generate the graphs are in supplementary File1/sheet 'figs3b'.

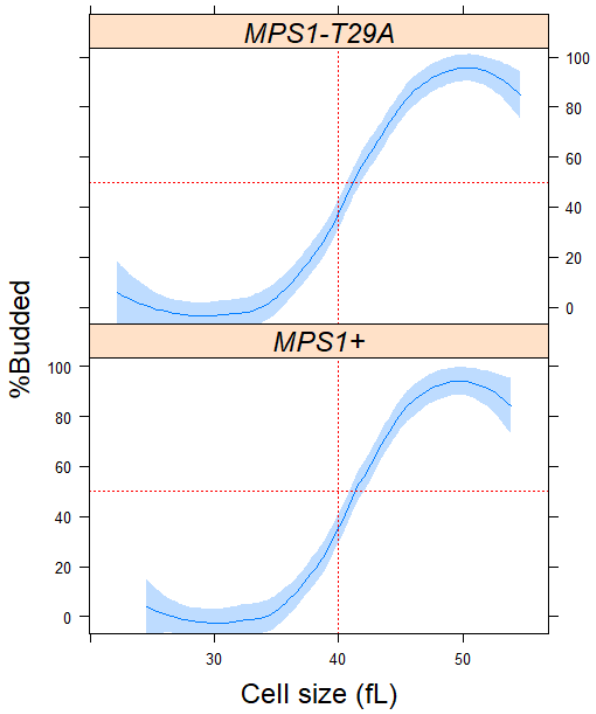

Figure S4. The timing of Start is not affected by introducing to Mps1p the T29A substitution that cannot be phosphorylated by Cdk. Summary of cell cycle profiles of the indicated strains, done as in Figure 2. Loess curves and the standard errors at a 0.95 level are shown. The values used to generate the graphs are in supplementary File1/sheet 'figs4'.

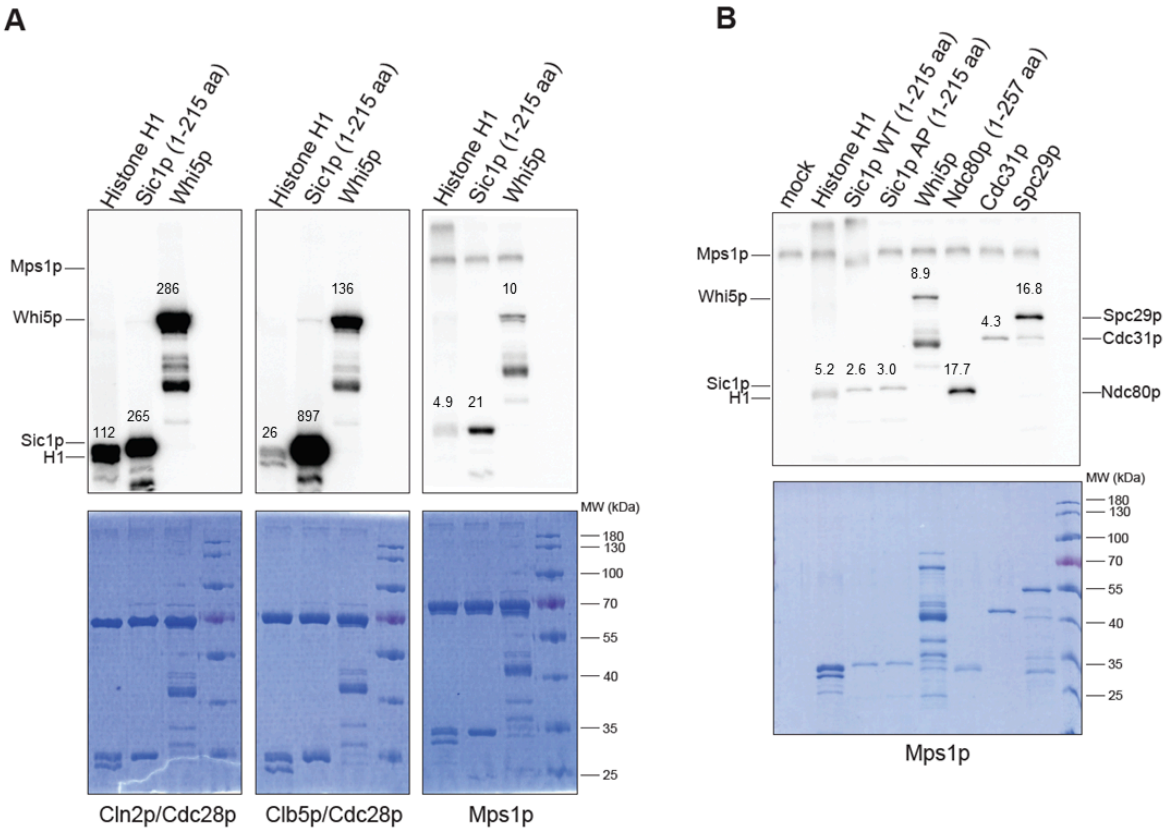

Figure S5. Mps1p can phosphorylate Whi5p and Sic1p in vitro. Autoradiograms of in vitro kinase reactions, displaying the incorporation of [^{32}P]-γ-ATP into the indicated substrates resolved on SDS-PAGE gels are shown top. The Coomassie-stained gels are shown below the autoradiograms. **A**, The kinases shown at the bottom were incubated with the substrates shown at the top for 16m, as indicated. **B**, Mps1p was incubated with each substrate shown at the top for 16m . The mock samples contain Mps1p alone. The numbers above the bands corresponding to each of the protein substrates are the relative quantification of the signal on each gel.